Geophysical study of the Ota–VF Xira–Lisbon–Sesimbra fault zone and the lower Tagus Cenozoic basin

2011 J. Geophys. Eng. 8 395

(http://iopscience.iop.org/1742-2140/8/3/001)

J. Geophys. Eng. **8** (2011) 395–411 doi:10.1088/1742-2132/8/3/001

Geophysical study of the Ota–VF Xira–Lisbon–Sesimbra fault zone and the lower Tagus Cenozoic basin

João Carvalho[1], Taha Rabeh[2,8,9], Miroslav Bielik[3], Eva Szalaiová[3], Luís Torres[4], Marisa Silva[5], Fernando Carrilho[6], Luís Matias[7] and Jorge Miguel Miranda[7]

[1] Laboratório Nacional de Energia e Geologia, Apartado 7586, 2721-866 Amadora, Portugal
[2] National Research Institute of Astronomy and Geophysics, Helwan, Cairo, Egypt
[3] Comenius University, Faculty of Natural Sciences, Mlynská dolina, 842 15 Bratislava 4, Slovak Republic
[4] LTGEO, Estrada do Paço do Lumiar 22, 1649-038 Lisboa, Portugal
[5] Instituto Geográfico Português, R. da Artilharia 107, 1099-052 Lisboa, Portugal
[6] Instituto de Meteorologia, Av. do Aeroporto, 2300-313 Lisboa, Portugal
[7] University of Lisbon, CGUL, IDL. Campo Grande, 1749-016 Lisboa, Portugal
[8] Geophysical Institute of the Slovak Academy of Sciences, Dúbravská cesta 9, 845 28 Bratislava, Slovak Republic

E-mail: taharabeh@yahoo.com

Received 2 November 2010
Accepted for publication 5 May 2011
Published 7 July 2011
Online at stacks.iop.org/JGE/8/395

Abstract

This paper focuses on the interpretation of seismic reflection, gravimetric, topographic, deep seismic refraction and seismicity data to study the recently proposed Ota–Vila Franca de Xira–Lisbon–Sesimbra (OVLS) fault zone and the lower Tagus Cenozoic basin (LTCB). The studied structure is located in the lower Tagus valley (LTV), an area with over 2 million inhabitants that has experienced historical earthquakes which caused significant damage and economical losses (1344, 1531 and 1909 earthquakes) and whose tectonic sources are thought to be local but mostly remain unknown. This study, which is intended as a contribution to improve the seismic hazard of the area and the neotectonics of the region, shows that the above-proposed fault zone is probably a large crustal thrust fault that constitutes the western limit of the LTCB. Gravimetric, deep refraction and seismic reflection data suggest that the LTCB is a foreland basin, as suggested previously by some authors, and that the OVLS northern and central sectors act as the major thrusts. The southern sector fault has been dominated by strike-slip kinematics due to a different orientation to the stress field. Indeed, geological outcrop and seismic reflection data interpretation suggests that, based on fault geometry and type of deformation at depth, the structure is composed of three major segments. These data suggest that these segments have different kinematics in agreement with their orientation to the regional stress field. The OVLS apparently controls the distribution of the seismicity in the area. Geological and geophysical information previously gathered also points that the central segment is active into the Quaternary. The segment lengths vary between 20 and 45 km. Since faults usually rupture only by segments, maximum expectable earthquake magnitudes and other parameters have been calculated for the three sectors of the OVLS fault zone using empirical relationships between earthquake statistics and geological parameters available from the literature. Calculated slip rates are compatible with previous estimates for the area (0.33 mm yr^{-1}). A more accurate estimation of the OVLS throw in the Quaternary

[9] Author to whom any correspondence should be addressed.

sediments is therefore of vital importance for a more accurate evaluation of the seismic hazard of the area.

Keywords: neotectonics, reflection seismology, gravimetric data, seismicity, seismic hazard

(Some figures in this article are in colour only in the electronic version)

1. Introduction

This paper focuses on the seismic hazard evaluation of the lower Tagus valley (LTV), sited in central-western Portugal mainland in the Eurasian Plate, close (about 200 km) to the Eurasia-Africa plate boundary (Azores-Gibraltar fault zone, figure 1(*a*)). This setting has resulted in significant tectonic and seismic activity throughout history (figure 1(*b*)). The study area includes the densely populated metropolitan Lisbon area, stressing the need to identify and characterize regional seismogenic faults as a condition for seismic potential assessment.

Besides the offshore sources, the study area suffers the effects of moderate events generated by local sources (Peláez *et al* 2002, e.g.) that also cause loss of life and significant damage like in 1344, 1531 and 1909 (Moreira 1985, Henriques *et al* 1988). The sources of these historical events are still under debate. Due to the scarcity of historical descriptions, the earthquakes in 1344 and 1531 are poorly located, being positioned in the LTV based upon the destruction generated in the Lisbon area. The 1531 event caused severe damage and many casualties in the town of Lisbon, reaching an intensity of VIII–IX MM (Justo and Salwa 1998).

The source of the $M_W = 6$ ($M_S = 6.3$) 1909 earthquake (Teves-Costa *et al* 1999, Dineva *et al* 2002), which destroyed the village of Benavente, is still unknown. The V. F. de Xira fault zone, or the southern, hidden sector of the Azambuja fault (AZF) is the nearest, NNE–SSW trending, candidates (Carvalho 2003, Cabral *et al* 2003, 2004). An alternative, as proposed by Stich *et al* (2005), is that the Benavente earthquake was generated by an ENE–WSW trending blind thrust beneath the Tagus valley sedimentary basin.

The geometry of the Cenozoic sedimentary basin also plays an important role in local energy enhancement and site effects, masking the relationship between the historical event location based on seismic intensity studies and the earthquake sources.

The correlation between instrumental seismicity and known active faults is also generally poor. The low slip rates indicate long recurrence times for maximum (M 6.5–7 co-seismic ruptures) earthquakes (about 2000–5000 years), evidencing the shortness of the historical record and stressing the need to refine the geological knowledge (neotectonic/paleoseismological).

However, fault recognition at the surface is often complicated due to the lack of outcrops and also due to the low slip rates in the study area, which causes sedimentation rates to erase surface ruptures. Therefore, faults are buried beneath the recent sedimentary cover and cannot be recognized at the surface. Even with well-located hypocentres, return periods are large in intraplate environments, and large earthquakes can be generated in previously undetected structures.

Therefore, the use of geophysical methods in the study area has been carried out in the last years in an attempt to improve knowledge regarding the deep structure, in particular the location and characterization of hidden faults, which may be the source of the regional seismicity (e.g. Cabral *et al* 2003, Vilanova and Fonseca 2004, Carvalho *et al* 2006, 2008). Reprocessing and reinterpretation of seismic reflection data acquired for oil exploration in the LTV and surrounding areas has been carried out, as well as of aeromagnetic (Carvalho *et al* 2008) and seismicity data (Carrilho *et al* 2004).

The Ota–Vila Franca de Xira–Lisbon–Sesimbra (OVLS) is one of the most important structures detected, based upon its near-surface expression on the seismic reflection profiles at several locations (Carvalho *et al* 2008), the remarkable signature it produces on aeromagnetic data (*id*; Domzalski 1969), its significance in the lower Tagus Cenozoic basin (LTCB) structural pattern, apparent relationship with the regional seismicity, its closeness to Lisbon and its foreseen seismic potential. Here, making use of gravimetric, topographic, deep-seismic refraction data and unpublished seismic reflection data, the importance of the OVLS as a crustal, regional boundary basin feature that can produce large earthquakes in the study area is proposed.

2. Tectonic and geological setting

The regional geodynamics is controlled by the NW–SE convergence of Eurasia and Africa at ∼4 mm yr^{-1} (NUVEL-1 model). Satellite geodesy indicates that the Eurasia–Africa motion changed significantly since ∼3 Ma (20° dextral rotation, 25–40% slowing). The present tectonic stress pattern in the study region has been assessed using various stress indicators (Ribeiro *et al* 1996, Borges *et al* 2001). While the nature of the Eurasia–Africa plate boundary in Ibero-Maghreb region is still a matter of debate (a diffuse border across the frontier between the oceanic and continental domains or a discrete but very complex plate boundary have been proposed), the level of seismotectonic activity in the West-Iberian continental margin indicates that it is not a typical passive margin.

A model suggesting that this margin is in transition from passive to active convergent has been proposed (Ribeiro *et al* 1996, Ribeiro 2002). In the last 15–20 years, data have been acquired offshore in the SW Iberian margin that revealed major NNE–SSW trending active faults. These faults confirm a model according to which the Iberian microplate is becoming individualized and is rotating clockwise between Africa and

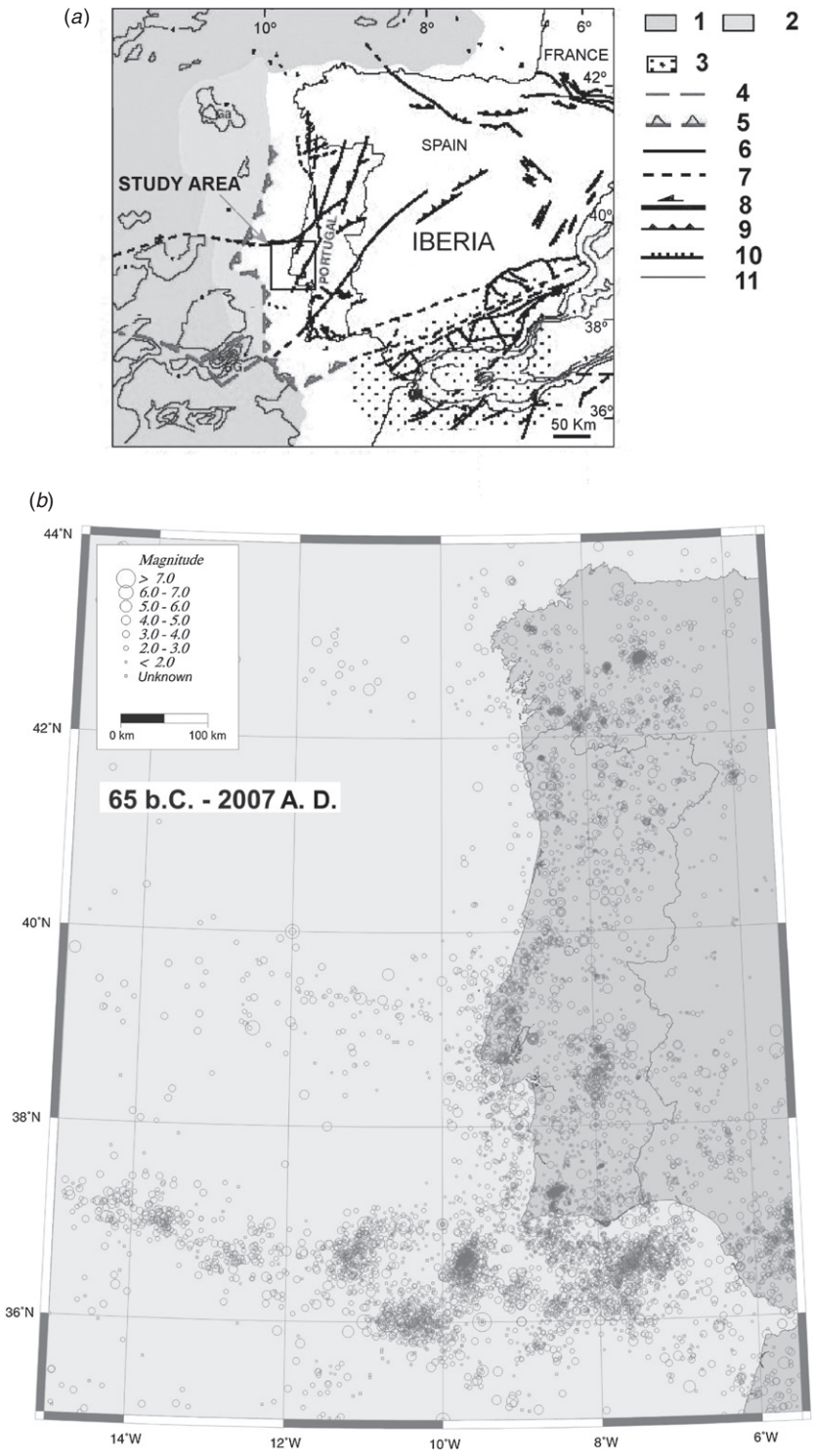

Figure 1. (*a*) Location of the study area and geodynamic setting (after Cabral 1995); (*b*) seismicity for the period 65 B.C.—2007 A.D. (source: Instituto de Meteorologia). (1) Oceanic crust; (2) transitional crust; (3) continental deformation area; (4) Eurorasia–Núbia plate boundary; (5) hypothetical subduction zone; (6) major fault zones; (7) probable faults; (8) strike-slip faults; (9) thrust faults; (10) normal faults; and (11) bathymetric contours.

Eurasia, inducing convergence across the West Iberia margin at $\sim$1 mm yr^{-1}.

The regional tectonic activity is expressed by crustal vertical movements and active faults that were reactivated with different tectonic styles, indicating a compressive regime. Average slip rates are usually $<$0.3 mm yr^{-1}, corresponding to a low to moderate degree of activity (Cabral and Ribeiro 1988, Cabral 1995, Carvalho *et al* 2006). As a consequence of this tectonic setting, mainland Portugal experiences a moderate seismicity, characterized by small events (M < 5.0) and occasional moderate to very large earthquakes, such as the well-known 1755 'Lisbon earthquake'.

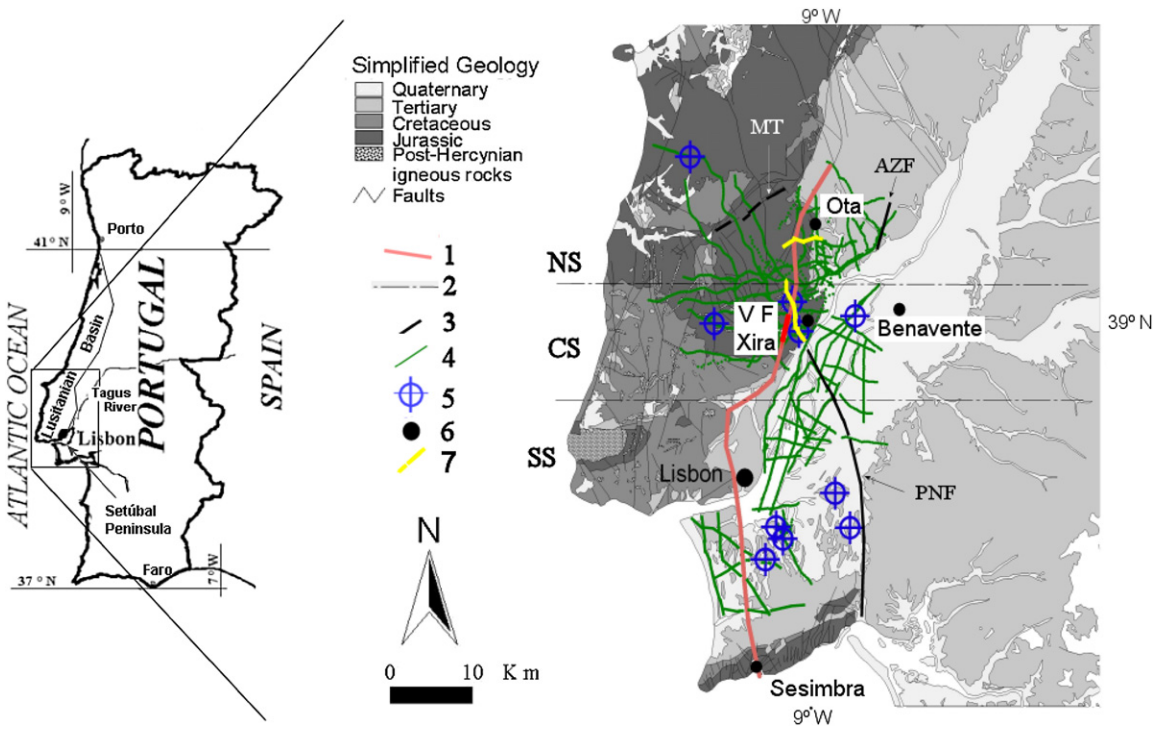

Figure 2. Simplified geological map (after Oliveira *et al* 1992) overlaid to the seismic reflection profiles and well data used in the upper Neogene structural mapping of the study area. The course of the OVLS inferred from potential field data is also shown. (1) Course of the OVLS fault zone inferred from potential field data; (2) delimitation of the OVLS segments; (3) faults discussed in the text; (4) seismic reflection profiles; (5) deep wells; (6) localities discussed in the text and (7) profiles shown in figure 3. AZF: Azambuja fault zone; PNF: Pinhal-Novo–Setúbal fault zone; MT: Montejunto thrust; NS: northern sector of the OVLS fault zone; CS: central sector; and SS: southern sector.

Using geophysical data, several other non-outcropping fault zones were mapped in the study area (e.g. Cabral *et al* 2003, Carvalho *et al* 2006). For some of them, such as the Vila Franca de Xira, Azambuja, Pinhal Novo faults, there is evidence from surface geology of tectonic activity since the Pliocene (Cabral *et al* 2003, 2004). Other structures are very probably active into the Quaternary: Porto Alto (Carvalho *et al* 2006) and central sector of OVLS (Vila Franca de Xira fault; Carvalho *et al* 2006, 2008, 2009).

The recently proposed OVLS fault zone (Carvalho *et al* 2008) shows three distinct segments with different behaviour, in conformity with their various orientations relative to the NW-SE maximum compressive stress. The northern segment splays into a series of NNE–SSW-oriented, east verging, imbricate thrusts which merge to the west into a major reverse fault that resulted from the tectonic inversion of the former normal fault bordering the Mesozoic Lusitanian basin (LB) in this area, the well-known Ota (or Pragança) fault. The central segment corresponds to the approximately 20 km long outcropping Vila Franca de Xira fault, which suffered a maximum degree of inversion. The southern segment, not recognized at the surface, extends for about 45 km, crossing Lisbon and the Setúbal Peninsula at depth until approximately Sesimbra (probably continuing offshore) with an N–S trend and distinct geometry. South of Vila Franca de Xira there is evidence for a WSW–ENE fault located at depth (Cabral 2009, Ribeiro *et al* 1990, Benavente fault, Carvalho *et al* 2008), producing a right-lateral stepover on the major structure, or possibly splitting the central from the southern segment.

In the study area outcrop Cenozoic sediments of the LTCB, a tectonic depression that surrounds the lower reach of the Tagus river, and the Mesozoic units of the Arruda sub-basin, which is part of the Mesozoic (LB) (figure 2). A description of the former basin can be found in Barbosa (1995) and Cabral *et al* (2003) while the evolution of the latter basin is described in Wilson *et al* (1989), Leinfelder and Wilson (1998), Rasmussen *et al* (1998), Carvalho *et al* (2005) and others.

3. Geophysical data set

3.1. Seismic reflection data

A few thousands of kilometres of seismic reflection profiles have been acquired for the oil industry since the mid 1950s until 1982 in the study area. These profiles were reprocessed recently and the quality of the stacks improved in most of the cases (see the location in figure 2). They have also been reinterpreted with OpendTect interpretation package. Several well logs and synthetic seismograms, VSP, aeromagnetic and gravimetric reprocessed data were used in the reinterpretation of the seismic profiles as well as recent geological information (Carvalho *et al* 2005). All these data were georeferenced and integrated in a GIS environment.

The identification of the major structures affecting the upper Neogene has been carried out by Carvalho *et al* (2006).

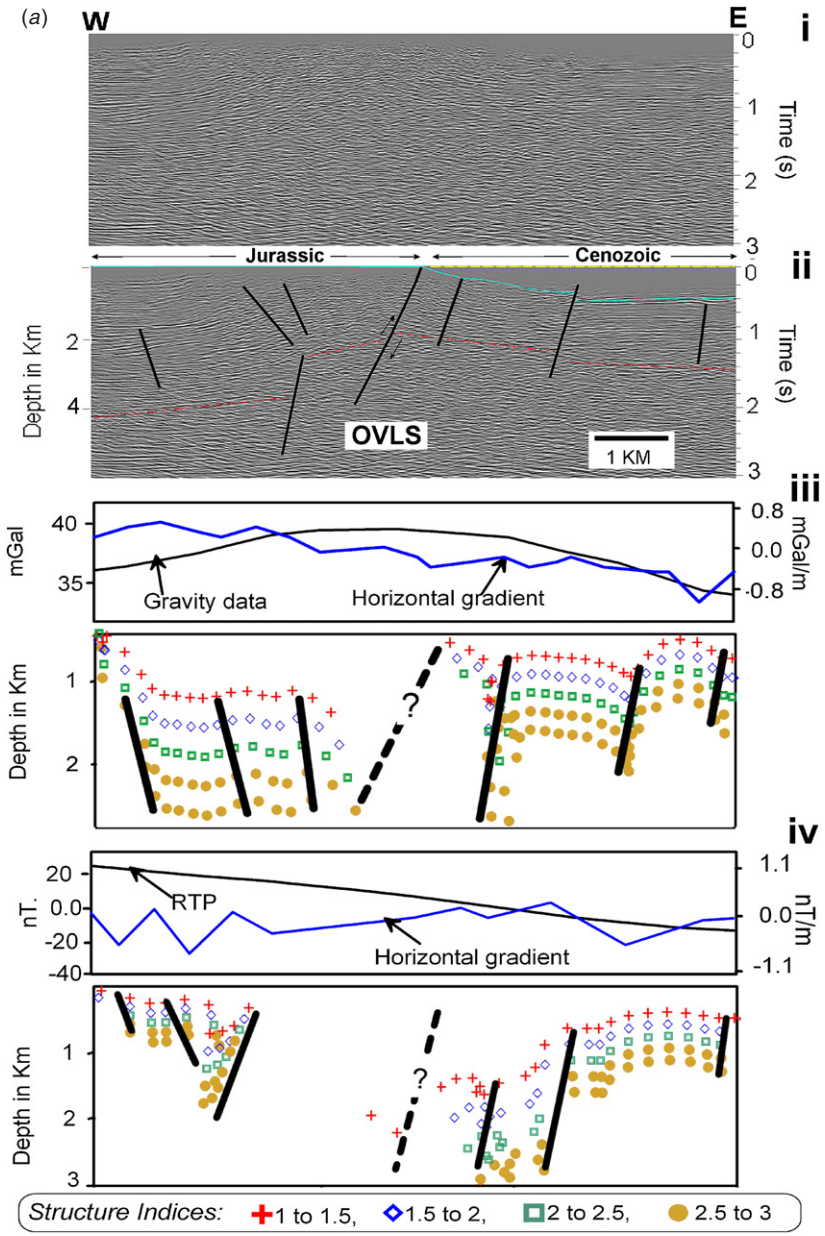

Figure 3. Examples of pre-stack time-migrated seismic reflection profiles (i) without and (ii) with interpretation overlaid (dashed line: Palaeozoic, continuous line: Mesozoic; dot-dashed line: Cenozoic); (iii) gravimetric and (iv) magnetic interpretations. Magnetic field is reduced to the pole (RTP). Magnetic and gravimetric interpretations techniques are (top panel) horizontal gradient of the RTP field (see section 3.2.1) and (bottom panel) 2D Euler deconvolution for a step function (see section 3.2.3). Profile 1 is located in the northern sector and profile 2 in the central sector (location on figure 2). Well's location is also shown (dotted line).

The faults were identified by visual inspection of the stacks using seismic attributes, by verifying fault consistency from line to line and the observation of 3D horizon structural maps. Potential field data were plotted over the seismic profiles and used to confirm major faults in the Mesozoic and Paleozoic rocks, as well as other geological structures, such as salt or igneous intrusions. The details of the reprocessing and interpretation of these data can be found in Carvalho (2003). Figure 2 also shows the course of the OVLS fault zone in the Paleozoic basement obtained from magnetic interpretation (Carvalho *et al* 2008).

Figure 3 shows examples of reprocessed and reinterpreted seismic reflection profiles located in the central and northern part of the fault zone (see the location in figure 2), with gravimetric and magnetic original interpretations overlaid. The latter interpretations were done independently of each other and also from seismic interpretations. Our preferred interpretation which is the seismic but final interpretation, overlaid on the seismic stacked sections, was achieved taking into consideration three methods. Faults were marked on the 2D magnetic and gravimetric cross-sections from the peaks of horizontal gradient analysis and discontinuities of 2D Euler deconvolution solutions for a step function.

These profiles show zones of chaotic reflections which have been associated with the Vila Franca de Xira fault outcrop (figure 3(*b*)) and Ota fault outcrop (figure 3(*a*))

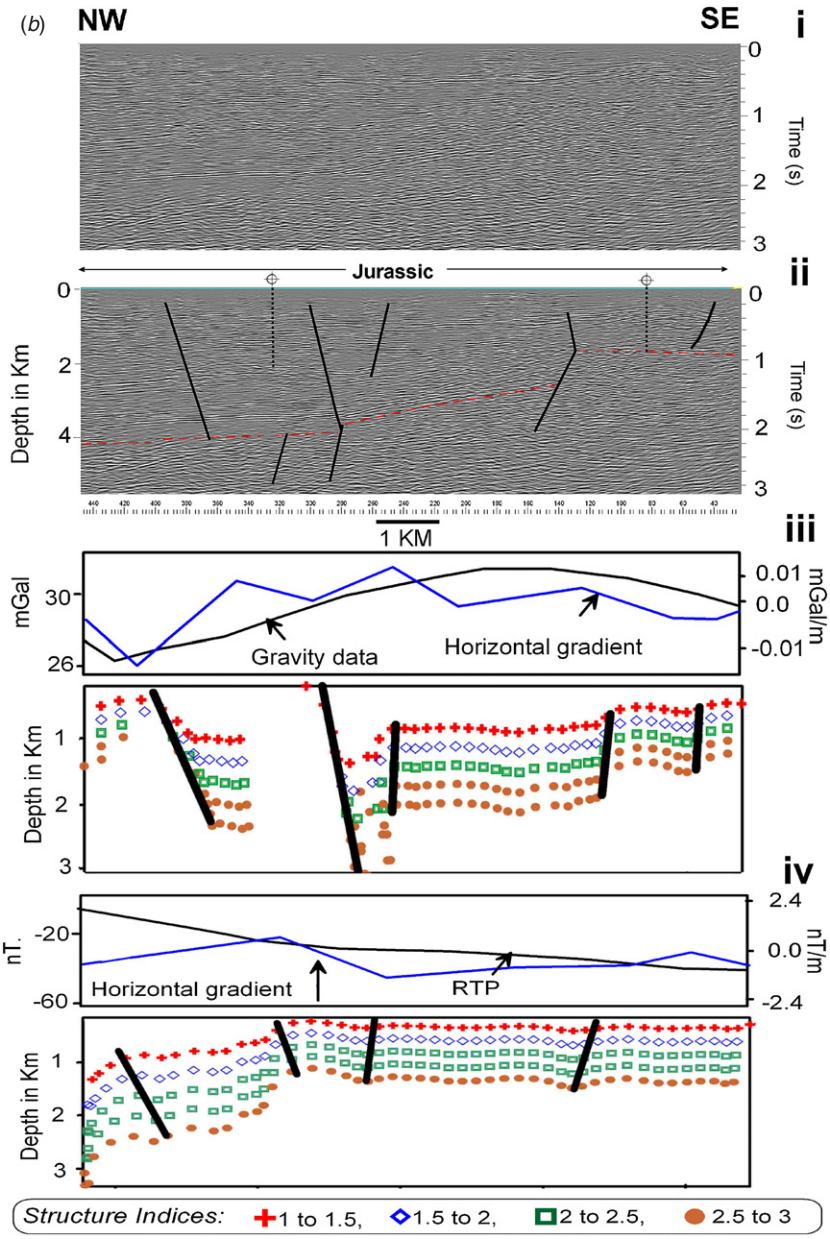

Figure 3. (Continued.)

(e.g. Wilson *et al* 1989, Leinfelder and Wilson 1998, Carvalho *et al* 2005). These faults constitute the central and northern sectors, respectively, of the OVLS fault system.

In spite of the better imaging capacities of seismic reflection data compared to potential field data, seismic imaging of a fault zone with an important strike-slip component might be difficult due to the large deformation produced by the fault and the resulting area of chaotic reflector pattern, which might also be caused by stratigraphic features, e.g. submarine fan, which is known to exist in the northern and central sectors of the OVLS (e.g. Wilson *et al* 1989, Leinfelder and Wilson 1998), close to the fault zone. Therefore, potential field data were used to locate eventual fault zones at depth (which also present a dip component) in the areas where both structural and stratigraphic features are possible.

Close to the edge of steep basement highs (which exist in part of all the three sectors of the OVLS; see e.g. figure 3), where low-fold seismic data also provide poorer imaging, combined gravimetric and aeromagnetic interpretation together with geological surface data provides valuable information regarding the existence of faults or paleo-relief.

3.2. Gravimetric data interpretation

A Bouguer anomaly map has been produced for Portugal mainland by joining different gravimetric surveys (L Torres, unpublished data). This map includes several campaigns acquired for ore prospecting by private companies and is an improvement of previous unofficial national gravimetric maps. The reference value used for the Bouguer correction was 2.67.

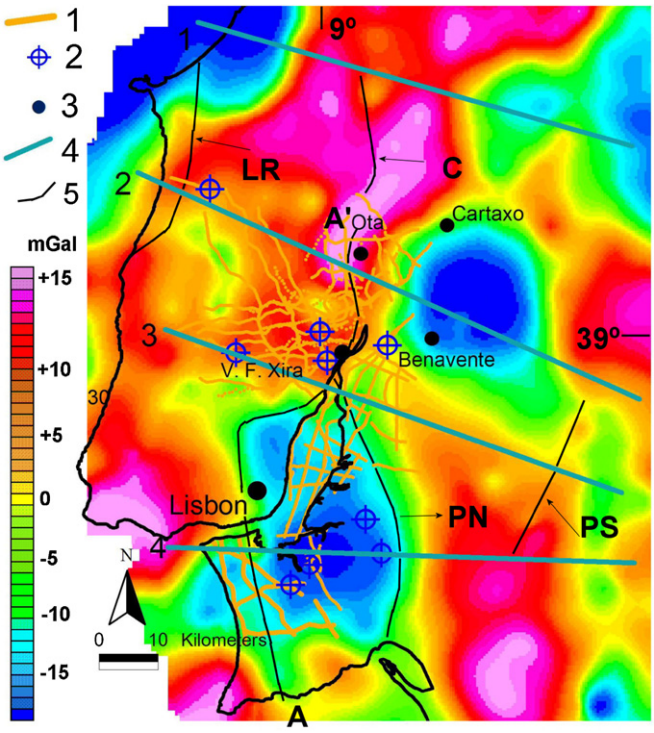

Figure 4. Second degree residual of the Bouguer anomaly map used in this work to assist the seismic reflection data interpretation and provide complementary information, particularly where no seismic data were available. A′–A: Course of the OVLS fault zone affecting the upper Miocene; C: cercal fault; PS: Ponte de Soure fault; PN: Pinhal Novo fault; LR: Lourinhã fault. (1) Seismic reflection profiles; (2) deep wells; (3) localities; (4) modelled regional profiles; and (5) faults.

Here, we have used a part of this map that covers the study area.

First- and second-degree polynomials were subtracted from the data in order to extract the regional trend. The subtraction of the second-degree polynomial produced a better separation of the anomalies, and this map (figure 4) was therefore used for the analysis and interpretation of the seismic reflection data. For interpretation of the gravimetric data, the original Bouguer anomaly map was used.

3.2.1. Construction of structural maps and regional setting for the study area. In order to detect the subsurface tectonic structures that affect the study area, the Bouguer anomaly maps were subjected to several analysis which were afterwards correlated with the results obtained from the seismic and previously carried out magnetic analysis (Carvalho *et al* 2008), with special emphasis on the OVLS fault zone. Since the metamorphic and igneous rocks that constitute the Paleozoic basement usually have a stronger magnetic signature than Mesozoic and Cenozoic sediments, we also expected to detect with the magnetic and gravimetric interpretation some structures affecting the basement which could not be imaged with the seismic reflection profiles.

For this purpose, these maps and sections were first submitted for several standard potential field interpretation techniques, such as gradient analysis, analytical signal and Euler deconvolution (section 3.2.3). Secondly, to provide a regional setting for the study area, in particular where no reflection data are available, a simple 2.5D modelling with constrains from seismic, well and outcrop data was performed (section 3.2.2). Finally, a stripping of the 3D effect of the Cenozoic layers in the Bouguer anomaly map was performed to provide insights into deeper Mesozoic and Paleozoic layers (section 3.2.4).

Grant and West (1965) and Linsser (1967) have published potential field data interpretation techniques that can be used to locate geological faults. The first horizontal gradient method was applied to the reduced to the pole (RTP) aeromagnetic and Bouguer anomaly maps. The peaks of the gradient curves were then plotted and connected to show possible structural alignments (not shown here), and this map was overlaid to fault maps obtained from seismic reflection and geological outcrop data.

In these aeromagnetic and gravimetric gradient maps, we can verify the occurrence of a regional structure which matches approximately the location of the OVLS fault zone, extending from the southern to the northern part of the studied area. It trends approximately N–S at the southern part and changes to a NNE–SSW direction in the north.

3.2.2. Two- and half-dimensional modelling. The potential field at a point with coordinates (x, y, z) due to an arbitrary volume of magnetic/gravimetric material can be expressed as (Surinkum 1989 modified from Talwani 1965)

$$A = 2KH[Px\ \cos 2\ I \cos 2D + Pz(\cos 2\ I \sin 2\ D - \sin 2\ I) + Q \cos D \sin 2I] \quad (1)$$

where Px, Pz, Q are the coordinates' parameters of the modelled body and can be calculated as follows:

$$Px = -\oint \frac{y}{r} - \frac{x^2}{x^2+z^2}\,\mathrm{d}_z; \quad Pz = -\oint \frac{y}{r} - \frac{x^2}{x^2+z^2}\,\mathrm{d}_x$$

$$Q = \oint \frac{y}{r} - \frac{x^2}{x^2+z^2}\,\mathrm{d}_x.$$

H is the earth's magnetic field strength and K is the magnetic susceptibility; D and I are the declination and inclination of the magnetic field, respectively.

In the case of gravity modelling, we substitute the magnetic field by the gravity field:

$$A = 2\ \rho\ G[Px\ \cos 2\ I \cos 2D + Pz(\cos 2\ I \sin 2\ D - \sin 2\ I) + Q \cos D \sin 2I],$$

where G is the earth's gravity field strength and ρ is the density contrast.

Computations of the gravimetric effects by models with complex geometry were carried out using commercial software (GM-SYS 1995). 2.5D gravimetric modelling was applied to a set of four profiles perpendicular to the strike of the gravimetric anomalies and covering the surveyed area (see the location in figure 4). The purpose of these long profiles is to provide a regional setting for the different sectors of the OVLS fault zone. The modelling was calibrated using seismic reflection and well data, where available, and geological outcrop data. The resulting modelled profiles are shown in figure 5.

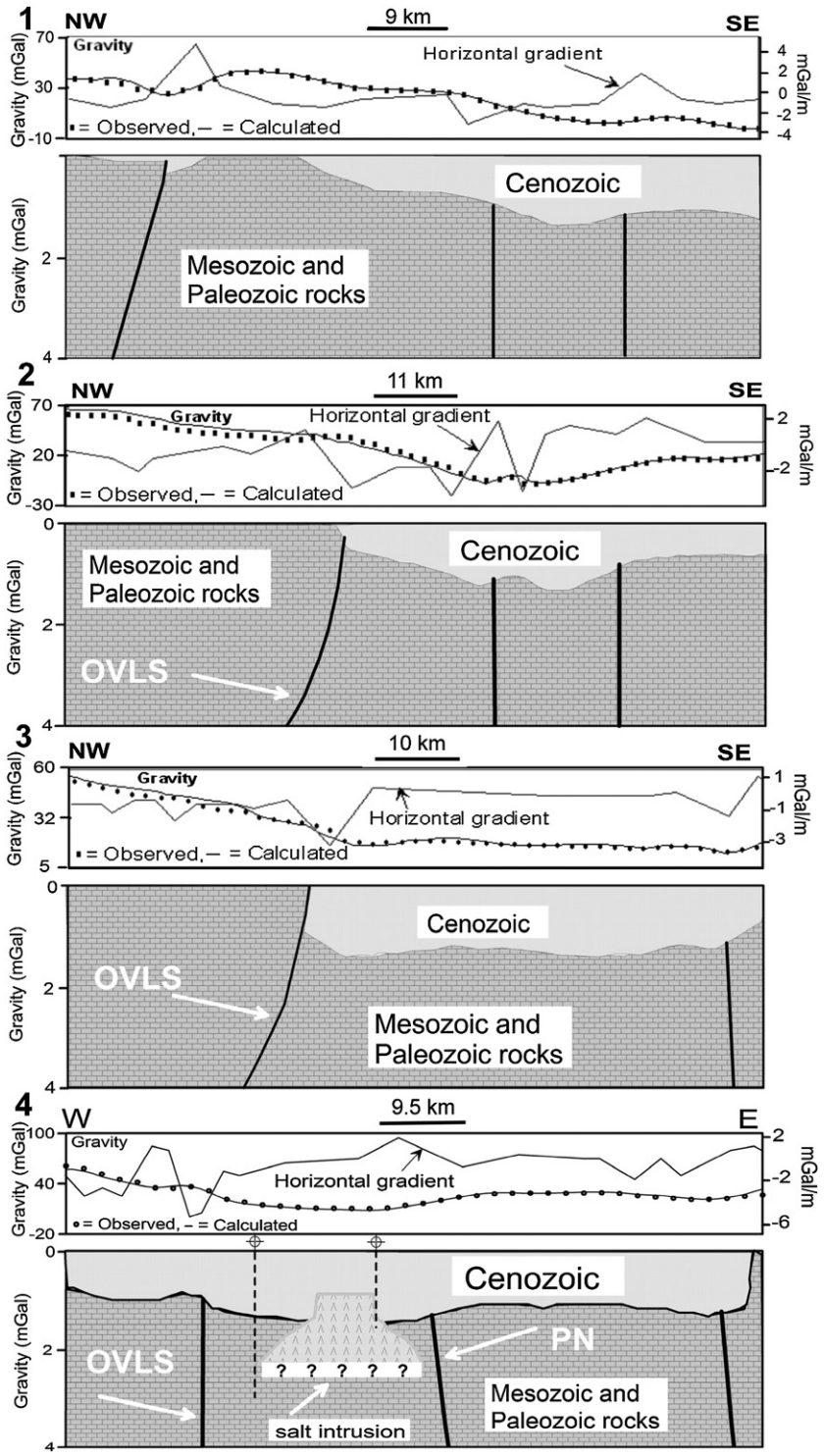

Figure 5. Profiles resulting from the 2.5D gravimetric modelling that provides a regional setting for the OVLS at its different sectors. The location of the profiles is given in figure 4. The black lines represent major geological faults. Their location was obtained from the peaks of the horizontal gradient of Bouguer anomaly, while fault geometry is obtained from seismic reflection and geological data. Wells that crossed the column of Cenozoic sediments are also indicated (dotted line). PNL: Pinhal Novo fault zone.

The main objective was to estimate the geometry of the top of the basement (Mesozoic units), and the presence of igneous structures or salt bodies, all interpreted as major contrasts in magnetization and density. In the area, Paleozoic igneous and metamorphic rocks form the magnetic basement. The gravimetric basement, according to well logs in the study and nearby areas is composed of jurassic carbonates and/or clastic units.

The depth to basement and location of igneous and salt bodies (but not faults, since these are our main target) were also analysed in all models from outcrop geological information, seismic reflection and well data, where available. Major faults

Table 1. Densities used in the forward modelling of the regional profiles presented in figure 5.

	Densities in g cm^{-3}					
	Basement rocks			Cenozoic sediments		
Profile	Maximum	Minimum	Mean	Maximum	Minimum	Mean
1	2.93	2.53	2.73	2.71	2	2.35
2	2.87	2.61	2.74	2.77	1.95	2.36
3	2.92	2.51	2.71	2.5	1.8	2.15
4	2.91	2.66	2.78	2.7	2.1	2.4

were also marked on the profiles (black lines in figure 5) from the peaks of the horizontal gradient of the Bouguer anomaly. The dip of the interpreted faults is based on geological and seismic reflection information where available.

The models show a distinct geometry throughout the study area. Mesozoic rocks, whose densities are only slightly inferior to average Paleozoic formations in the area, while the Cenozoic units present much lower densities, here compose the gravimetric basement. Therefore, gravimetric modelling is well suited to detect the shape of the Tertiary basins of the study area, such as the LTCB. The densities used in the direct modelling are listed in table 1.

3.2.3. Euler deconvolution method. The Euler deconvolution method (Reid *et al* 1990) aims at determining the positions and depths of the sources of the magnetic or gravimetric contrasts. Thompson (1982) showed that the relation of Euler's homogeneity could be written in the form

$$(x - x_0)\partial F/\partial x - (y - y_0)\partial F/\partial y + (z - z_0)\partial F/\partial z = N(B - F), \tag{2}$$

where (x_0, y_0, z_0) is the position of the potential field source whose total field F is detected at (x, y, z). The total field has a regional value of B. The degree of homogeneity N may be interpreted as a structural index (SI), which is a measure of the rate of change of the field with distance. For the index of sloping magnetic contact, the appropriate form of Euler's equation is

$$(x - x_0)\partial F/\partial x - (y - y_0)\partial F/\partial y + (z - z_0)\partial F/\partial z = A, \tag{3}$$

where A incorporates amplitude, strike, and dip factors which cannot be separated easily.

This technique, which is often applied to gridded data, measures the gradients, locates the square windows of the potential field and respective gradient values, and determines structural windows. The results can be plotted in map view or cross-section using a symbol related to depth z.

The Euler deconvolution technique was also applied to the vertical gradient of the gravity data to provide an improved source resolution (Stavrev 1997, Hsu 2002) as shown:

$$\frac{\partial}{\partial x}\left(\frac{\partial^n f}{\partial z^n}\right)(x - x_0) + \frac{\partial}{\partial z}\left(\frac{\partial^n f}{\partial z^n}\right)(z - z_0) = SI\left(\Delta\left(\frac{\partial^n f}{\partial z^n}\right) + B_z\right), \tag{4}$$

where n is the order (which is not necessarily an integer (Cooper and Cowan 2003) of the gradient used. It may similarly be applied to the horizontal gradient as shown:

$$\frac{\partial}{\partial x}\left(\frac{\partial^n f}{\partial x^n}\right)(x - x_0) + \frac{\partial}{\partial z}\left(\frac{\partial^n f}{\partial x^n}\right)(z - z_0) = SI\left(\Delta\left(\frac{\partial^n f}{\partial x^n}\right) + B_x\right). \tag{5}$$

In a previous work we had applied the method to plan view gridded magnetic data with good results (Carvalho *et al* 2008). In this work we applied the Euler deconvolution to gridded gravimetric data but unfortunately the latter does not have the required resolution to produce adequate results.

This technique was also applied to the gravimetric and aeromagnetic data in the form of 2D profiles and the faults inferred from seismic data overlaid. The Euler deconvolution method has been applied using 0.5 gravimetric and magnetic step indices, in order to indicate the depth to the basement rocks and their structures.

The gravimetric and magnetic Euler solutions using the gradient method produced good results along profiles (see examples in figure 3), presenting in some cases a good correlation with the fault locations deduced from seismic reflection interpretation, while in others, the lower spatial resolution of the gravity survey did not allow a good match between the various techniques. A discussion on the interpretation of gravity, and magnetic and seismic 2D profiles is presented in section 4.

3.2.4. The stripped gravity map. The so-called stripped gravity map (SGM) (Hammer 1963, Bielik 1988a) is used for the calculation of the regional gravity anomalies that are due to density inhomogeneities located beneath the basement of the basin. It is constructed by removing from the Bouguer gravity map the gravity effect of the sedimentary infill. Generally, young (Cenozoic) basins are composed of unconsolidated sediments, which are characterized by low density values that originate short-wavelength negative gravity anomalies. These near-surface anomalies obscure the longer wavelength (regional) gravity effects of deeper-seated density anomalous bodies (Bielik 1988a, 1988b).

This technique is therefore well suited for the geophysical study of deep structures in the studied region, which is covered by a highly variable thickness of Neogene sediments (from 0 to about 2.4 km). The process of calculation of the SGM is based on the determination of the 3D gravity effect of the sedimentary infill of the basin (Bielik 1988a, 1988b, Bielik *et al* 2004, 2005).

The 3D numerical gravity modelling is a very convenient method for the interpretation of the gravity field. The gravity effect of the low-density sediments is calculated by an algorithm developed by Starostenko *et al* (1997). The geological structure is approximated by an n-sided vertical prism, which is limited by an arbitrary relief of the upper and lower boundaries (Starostenko *et al* 1997, Legostaeva 2000). The 3D density model consists of unconsolidated Cenozoic clastics, occasionally intercalated with thin calcareous sandstone layers.

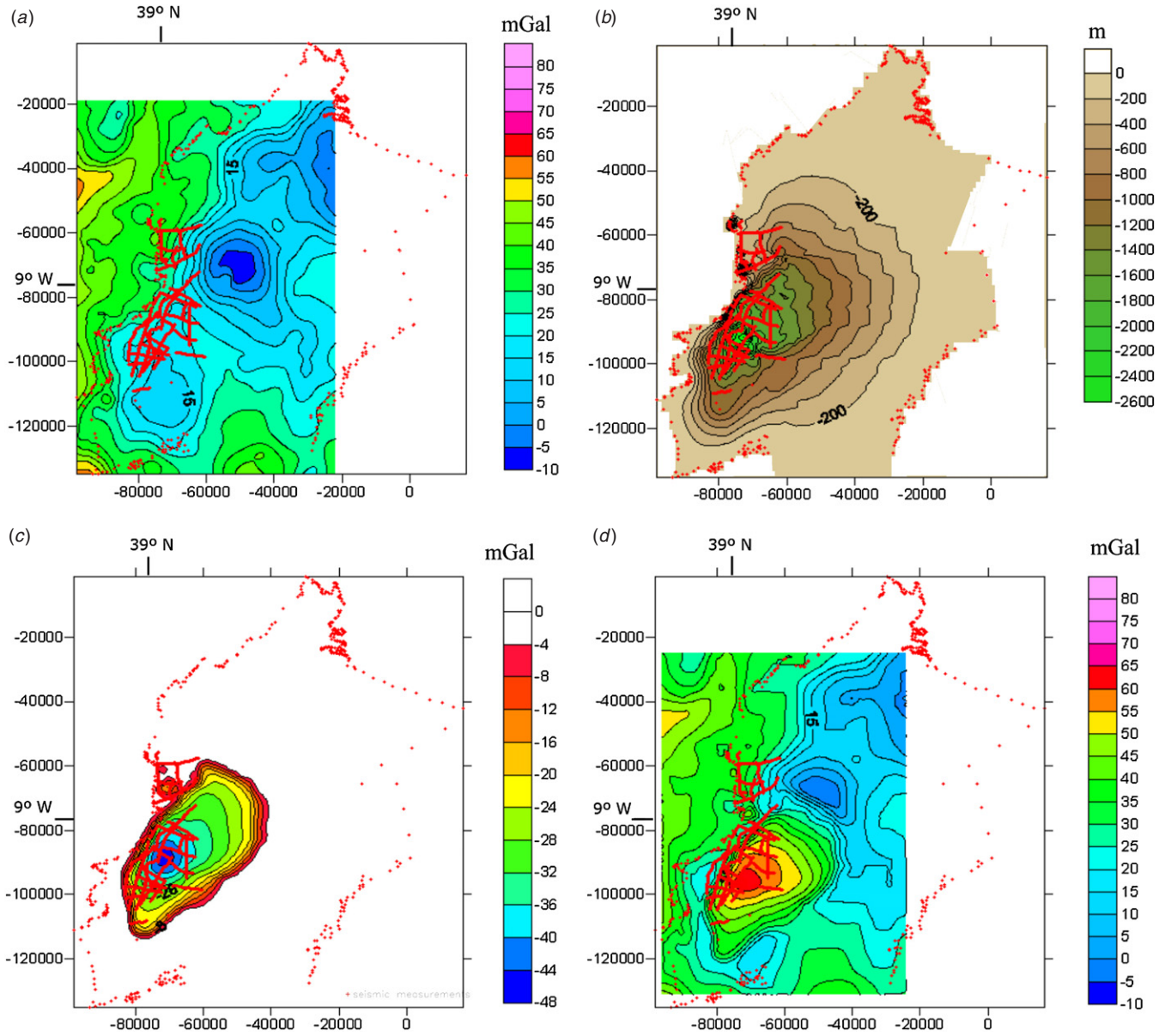

Figure 6. Major steps necessary to produce the SGM: (*a*) Bouguer anomaly map (for a density of 2.69); (*b*) base of the Cenozoic map built from seismic reflection, well and geological outcrop data; (*c*) gravity effect produced by these units; (*d*) SGM resulting from the subtraction of (*c*) from (*a*). The red dots indicate the locations where the depth to the base of Cenozoic was available.

The base of the Cenozoic sediment map was constructed using seismic reflection, geological outcrop and well data (Carvalho *et al* 2005). Since the seismic profiles were limited only to the western and central part of the LTCB, information about the basement relief in the whole basin had to be extrapolated. In the northern part of the study area, the accuracy of this extrapolation is in agreement with the modelling carried out in section 3.2.2 (figure 5) and geological information (Barbosa 1995). The extrapolation to the east, on the other hand, is in agreement with the interpretation of seismic reflection and refraction profiles located a few tens of kilometres east of the profiles reprocessed here (Westerhausen 1956) and geological information, which suggests a relatively smooth up-rise of the base of Cenozoic to the east until close to the generalized outcrop of Paleozoic rocks. Here, as suggested by the modelling presented in figure 5 (profiles 4 and 3), one (or more) fault(s) bring the Palaeozoic to the surface. The location of this fault is close to the limit of the model and produces negligible effects on the calculated 3D gravity effect of the Cenozoic sediments.

The largest thickness (up to 2.4 km) of Cenozoic sediments can be observed in the central part of the basin. An average density of 2.2 g cm^{-3} for these sediments was determined from unpublished well data available at the National Laboratory for Energy and Geology (LNEG), GPEP (1986) and Carvalho *et al* (2005). Densities of 2.3 and 2.4 g cm^{-3} were also used. For Mesozoic and Paleozoic units, the average (reference) density is 2.75 g cm^{-3} (Carvalho *et al* 2005). This means that we used an average density contrast of 0.55 g cm^{-3} for our 3D model. The Bouguer anomaly, base

of Cenozoic, gravimetric effect of Cenozoic units and SGMs are shown in figure 6.

A striking outcome of this map is a strong positive anomaly located at the lower Tagus estuary. The amplitude of this anomaly is reduced when higher densities are used for the sedimentary Cenozoic infill but its shape and presence remained. We emphasize that the obtained SGM is conditioned by the thickness of the Cenozoic sedimentary infill, leading to this rather localized positive anomaly where the thickness of sediments is more than 2 km. It is expected that if the strong negative anomaly located further north is also partially caused by a thicker Cenozoic column as is the one over the Tagus estuary (this is suggested by an unpublished deep refraction line acquired in the 1950s (Westerhausen 1956) and by seismic reflection line ar8–81 located at the border of this anomaly), this correction of the base of the Cenozoic map will produce a spatial enlargement of the referred positive anomaly that will be in better agreement with the shape of the LTCB.

3.3. Deep seismic refraction data and digital terrain model

In order to obtain information from the structure of the study area and assess the presence (or not) of the OVLS fault zone at depth, deeper crustal data were required. Such data have been collected in Portugal mainland since the 1970s from deep refraction profiles (e.g. Mueller *et al* 1973, Moreira *et al* 1980, Mendes-Victor *et al* 1980 and reinterpreted by Matias 1996).

One of these profiles, whose location is shown in figure 7(*a*) (P1–P2), is well suited for the above purpose. It has a NW–SE trend and crosses the central sector of the OVLS fault zone and passes about 40 km NW of the SGM's positive anomaly over the Tagus Estuary. The deep refraction model (Matias 1996) is presented in figure 7(*c*). It can be observed that the shape of the LTCB (figure 7(*c*)) is in good agreement with the structure deduced from the gravimetric modelling calibrated by seismic reflection and well data (compare profile 2 of figure 5 with profile P1–P2 from figure 7(*c*), which have an approximate location). Figure 7(*b*) also shows a general model of a foreland basin (after Cobbold *et al* 1993).

A shaded relief map obtained from a digital terrain model (DTM) with a ground sample distance of 25 m is shown in figure 8. The DTM was constructed using altimetry information from the national map M7810, at a 1:50 000 scale. The shaded relief map of the study area was used to correlate with other sources of data, since it is well known that though geological structures often produce topographic features, some other topographic features can be attributed to differential erosion, transgressive/regressive episodes, hydrographical network and others. In figure 8 we have overlaid major possible seismogenic faults inferred from seismic reflection, potential field and geological outcrop data.

Although the topographic control might be active or passive from a neotectonic point of view, the consequences of the presence of the central and northern sectors of the OVLS fault zone are clearly seen. In its northern and central sectors, the western block of the fault zone, composed of rugged, fractured Mesozoic rocks, clearly differentiates

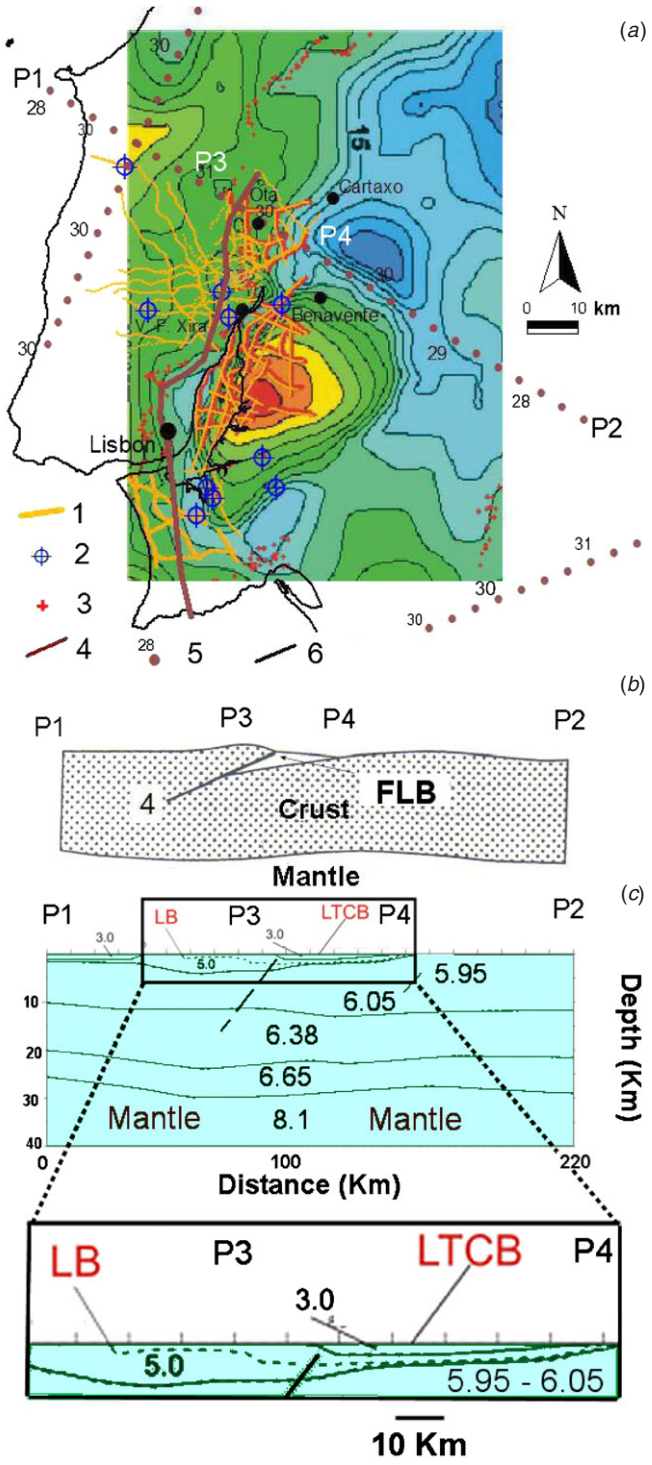

Figure 7. (a) Location of the profiles where deep seismic refraction data were acquired overlaid on the SGM: (1) seismic reflection profiles; (2) wells; (3) data used in the construction of the base of the Cenozoic map; (4) OVLS fault zone course; (5) deep refraction profiles with estimated Moho depths indicated; and (6) coastline. (*b*) General model of a foreland basin after Cobbold *et al* (1993). FLB: foreland basin; 4: major deep-rooted thrust. (*c*) Velocity model obtained by interpretation of the refraction data (after Matias 1996). Numbers represent average P-wave velocities. The black line represents the location of the OVLS fault zone (compare with 4 in (*b*)).

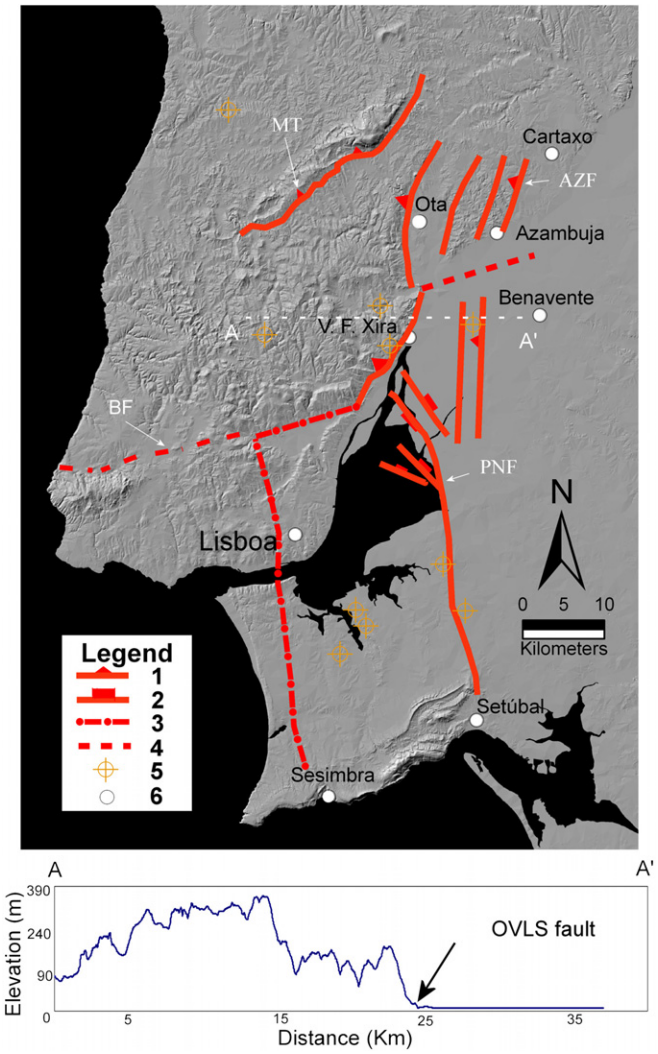

Figure 8. Top: DTM model and major hidden, possible seismogenic faults affecting the study area (see the legend of figure 2). A–A′: Topographic profile shown at the bottom of the figure. (1) Reverse fault (marks on upper block); (2) normal fault (marks on lower block); (3) inferred fault from potential field data; (4) probable fault; (5) wells; and (6) localities. BF: Benavente fault zone. Bottom: topographic profile over the central sector of the OVLS fault zone (location of the fault is indicated).

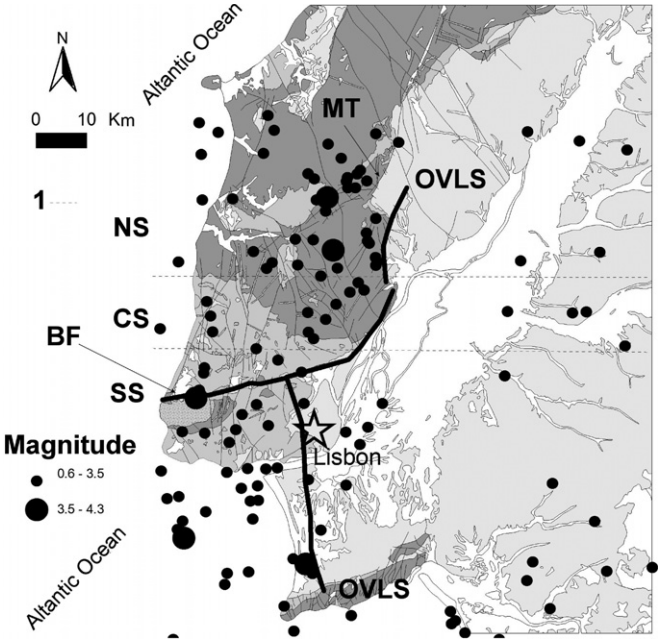

Figure 9. Relocated seismicity after Carrilho *et al* (2004) for the period 1970–2000 and relationship with the OVLS, Benavente (BF) and Montejunto thrust (MT) fault zones, showing the control of the former structure in the seismicity distribution. Geological contours shown in figure 2 are also overlaid. (1) Geographical delimitation of the OVLS segments. NS, CS, SS: northern, central and southern sectors, respectively.

from the flatter, smoother Quaternary and Tertiary formations that compose the eastern block. Here, extensive Holocenic alluvia deposited in the last 15 kyears, erasing any eventual topographic features resulting from a low-slip-rate tectonic activity.

In the southern sector at the South of Lisbon (Setúbal Península), the fault zone is no longer recognizable from a topographic point of view. This fact maybe explained by the different orientation of the fault zone relative to the stress field during the Miocene (Ribeiro *et al* 1996), favouring a dominant strike-slip movement rather than the predominantly reverse dynamic of the northern and central sectors. The strike-slip component of this fault zone is suggested by seismic reflection data (see figure 3 (*e*) from Carvalho *et al* 2008) that show a sub-vertical fault with a minor rise of the western block.

The WSW-ENE fault zone (Cabral 2009, Ribeiro *et al* 1990) recently called the Benavente fault (Carvalho *et al* 2008) has also a clear topographic signature on the western margin of the Tagus (BF, figures 8 and 9). On the eastern margin, where the already mentioned Quaternary and Holocenic deposits predominate, its hypothetical prolongation across the Tagus (where it would cross close to Benavente) or any other coherent or significant feature which may be associated with tectonic episodes is not recognizable.

One of the two other outstanding features of the DTM map is the Montejunto fault zone, located at the north of the map and which according to surface geological data is a reverse fault with a left-lateral strike-slip component (Ribeiro *et al* 1990, Cabral 1995) and is thought to be an active structure (e.g. Curtis 1999). The other is the northern limit of the Arrábida chain, sited in the south of the study area, which was created by S-verging thrusts along a low-dip fault (probably installed in a Hettangian evaporite complex during the Miocene (Ribeiro *et al* 1990). It separates Tertiary sediments at the north from Mesozoic formations at the south. Other active faults are visible in the map, such as the SSW–NNE AZF, located near Cartaxo (figure 8).

Several other topographic features visible in the Mesozoic terrains are associated with differential erosion or other faults, which may not have been active in recent times. Some of these structures have very few Quaternary type of sediments along their course, and it is difficult to determine if they had movement during the last 1000 kyears.

4. Seismicity

Relocated epicentres from the period 1970–2000 (Carrilho *et al* 2004) using the software Hypocent (Lienert *et al* 1986, Lienert and Havskov 1995) are plotted in figure 9. The average error (90% confidence level) in the epicentral locations is 5 km. The OVLS fault zone course proposed in this paper, inferred from seismic reflection and potential field data, is also shown in figure 9.

The vast majority of earthquakes are located to the west of the fault course in the three sectors, in agreement with the model of a foreland basin where most of the deformation occurs in the upthrust block. In the northern sector, at the northern part of the study area, there is also a clear correlation between the Montejunto thrust and seismicity (please compare figures 8 and 9) which strongly suggests that it is an active structure, as already recognized by Cabral (1995) and Curtis (1999), for example.

In the northern and central sectors of the OVLS, to the east of the fault zone course there is a N–S-oriented gap in seismicity of about 20 km long. The events at the far east of the figure after the gap cannot be correlated with any known active faults (no coverage of seismic reflection data in this area).

In the southern sector, there is also a relative gap in seismicity at the east of the OVLS fault but about ten events are located close to the fault plane. About five to six of these events make an alignment that can be associated with a large structure deduced from Landsat data (Cabral and Ribeiro 1988, Cabral 1995) but which was found later not to affect Cenozoic sediments (e.g. Cabral *et al* 2003): the LTV fault (Cabral and Ribeiro 1988). The reprocessing and reinterpretation of seismic reflection data carried out in this work suggests the existence of this structure at depth, in Mesozoic terrains. The other events located further east in this sector cannot be associated with known active faults as well.

Furthermore, in spite of poor hypocentral solutions, the distribution in depth of the seismicity in the area can apparently be associated with the OVLS fault plane. Figure 10 shows tentative depth sections for the three sectors where the instrumental seismicity (Carrilho *et al* 2004, see above) is overplotted to the OVLS fault plane prolonged at depth in agreement with seismic reflection data in the upper kilometres. The images have been rotated around the depth axis in order to make the fault plane perpendicular to the angle of view, to allow a better association between the fault zone and hypocentres.

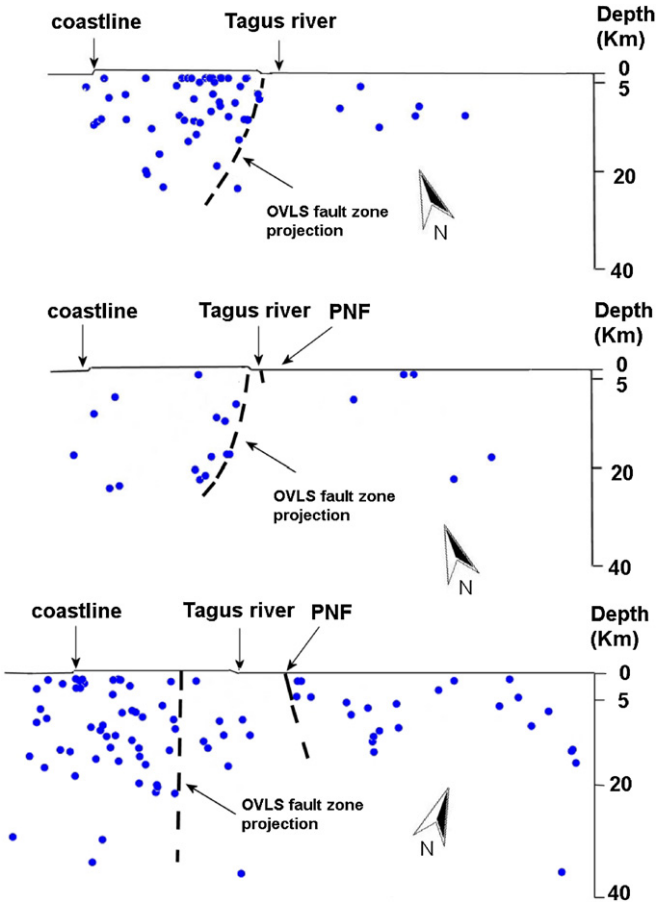

Figure 10. Relocated epicentre data from figure 9 plotted in depth with inferred projection of the OVLS fault plane for the three sectors. Images have been rotated in turn of the *Z*-axis to make the fault plane approximately perpendicular to the angle of view. Dips of the fault zone in the upper few kilometres are inferred from seismic reflection data. PNF: Pinhal Novo fault zone.

5. Discussion

The gravimetric and magnetic interpretations shown in figure 3 are, in some cases, slightly different from each other, but if we take into consideration the response of the two different methods, this discrepancy can be explained. In the latter, the Mesozoic rocks (2.6 g cm^{-3}) or Palaeozoic rocks (2.8 g cm^{-3}) constitute the gravimetric basement, since Cenozoic layers are clearly less dense (around 2.2 g cm^{-3}). Therefore gravimetry is appropriate to study Cenozoic basins, e.g., and in the areas where these sediments are not present, it provides insights into Mesozoic and Palaeozoic rocks. Magnetics responds mostly to metamorphic and igneous Palaeozoic rocks. It is also well known that magnetics is more sensible to lithological variations than gravimetry.

This means that we are imaging not exactly the same layers with the two methods. Also, as the faults propagate upwards, they change their dips, and this is quite common particularly with reactivated faults (in the study area, Palaeozoic thrusts were often reactivated as normal faults in the Mesozoic and the latter reactivated as thrusts during Cenozoic tectonics). Therefore, it is not surprising that we do not 'see' the same structures with the two methods, and an integrated interpretation with seismic reflection and geological outcrop data is essential for a better understanding of the tectonics of the area.

Taking into consideration what is said in the above paragraphs, magnetic data should provide insight into greater depths. However, if we compare the Euler deconvolution solutions for gravity and magnetics, the former is able to image greater depths. This result may be connected with the resolutions of the magnetic and gravimetric surveys, the latter with less spatial resolution, and therefore containing more

long-wavelengths, and the physical nature of the technique applied (Euler deconvolution to vertical gradient of the field).

The gravimetric models obtained by 2.5D modelling complement previously published magnetic models since, as stated above in this section, gravimetry and magnetics respond to different properties of the subsoil. The models of the gravimetric profiles presented in figure 5 show with simplicity several aspects of the regional structure of the study area. The model of profile 1 shows that the LTCB has a maximum thickness in this area of about 1.4 km, and this local depocentre is located to the NE of Cartaxo, close to the river Tagus. The average thickness of the basin here is less than 1 km. The border between the Mesozoic LB and the LTCB in this area, according to geological outcrop data (LNEG 2010), is not affected by faulting, but a few kilometres further north a reverse fault with the upthrust block located to the NW has been mapped (LNEG 2010). The northwestern fault shown in this profile modelling clearly correlates with a mapped fault (LNEG 2010) related to the Óbidos and Caldas da Rainha diapirs. The two easternmost faults that are visible in the model do not correlate with known outcropping faults.

Profile 2, crossing the northern sector of the OVLS fault zone, shows that the thickness of the Cenozoic sediments is very similar to that of profile 1, while the contact between the LB and the LTCB here is clearly associated with the OVLS fault zone. The DTM shown in figure 8 demonstrates the upthrust of the western block, in agreement with seismic reflection data interpretation presented here (figure 3(*a*)) and by other authors (e.g. Rasmussen *et al* 1998) that the Pragança (or Ota) fault, a previously normal fault, was inverted in Cenozoic times.

Profile 3 (figure 5(*c*)) shows that the OVLS fault zone presents the greatest expression here, evidencing a much larger vertical displacement. This agrees with geological information that indicates the strongest degree of inversion in the central sector. Here the LTCB average depth is larger (around 1.2 km) than in the northern part but the maximum thickness is similar (about 1.4 km).

Further south, in the Setúbal Peninsula, profile 4 (figure 5(*d*)) evidences that the southern segment of the OVLS fault zone produces a much reduced vertical displacement in the Mesozoic gravimetric basement when compared to the central sector, while seismic data suggest a larger vertical offset in the Palaeozoic rocks (see figure 3(*e*) from Carvalho *et al* 2008).

Though this fault may probably have been a pre-inversion fault, seismic data show that it was not the Mesozoic basin boundary fault zone (no significant growth is observed in Jurassic sediments), as were the faults of the northern and central segments. Profile 4 also suggests the presence of a large mass of salt in agreement with well Pinhal Novo 1 (see the location in figure 5(*d*)) that detected a salt diaper at a depth of about 900 m (e.g. GPEP 1986, Rasmussen *et al* 1998). The maximum depth of the LTCB in this sector is around 1.4 km and similar to other parts of the basin, but the average thickness to the west of the OVLS is clearly less than to the east of this fault and in other parts of the basin in agreement with seismic data (see also figure 3(*e*) from Carvalho *et al* 2008).

Consequences of the geological inversion geologically observed at the central and northern sectors of the OVLS fault zone can be observed in the DTM: the presence of rugged, fractured, Mesozoic rocks on the western upper block of the fault and the smooth plain Cenozoic terrains of the eastern block. The fault course can be clearly identified in the DTM (see figure 8), except in the Península of Setúbal (the southern part of the southern sector of the fault zone).

Seismicity data presented here support that the OVLS reaches crustal depths (figure 10). The model obtained from deep refraction data interpretation shows that we have a thicker crust to the west of the OVLS fault zone and a thinned crust to the east, below the LTCB basin. This model agrees with a general model of a foreland basin (figure 7(*b*)) where the OVLS would be its western limit and accommodate major thrust deformation.

However, an alternative tectonic model can also produce crustal thinning below the LTCB: a pull-apart basin. In this case, the thinning of the crust would be caused by the stretching produced by two large strike-slip faults (e.g. Dooley *et al* 2007). In the LTCB case, these two fault zones would be the OVLS (central sector) which has a recognized important left-lateral strike-slip component (Ribeiro *et al* 1990, Cabral *et al* 2003, Vilanova and Fonseca 2004) and the left-lateral Pinhal Novo–Setúbal fault (Ribeiro *et al* 1990, Cabral *et al* 2003, Vilanova and Fonseca 2004).

However, this pull-apart basin model should produce a thinned crust between the two major fault zones and not to the north of the Pinhal Novo–Setúbal fault, where we have the deep refraction profile (P1–P2 of figure 7) which shows a thinned crust. The pull-apart basin model also requires strike-slip sub-vertical faults. However, seismic data suggest that the OVLS curves at depth in the northern and central sectors (see figure 3 of this paper and figure 3 from Carvalho *et al* 2008). This curvature is also suggested by hypocentre data (figure 10). The Pinhal Novo–Setúbal fault zone also presents some curvature according to some authors (e.g. Cabral *et al* 2003). Seismic stratigraphy and available well data suggest a rapid accumulation of sediments during the Miocene (e.g. Cabral *et al* 2003) which further suggests the foreland basin model for the LTCB.

The acquisition of deep seismic reflection data across the basin, similar to what has recently been done in the Iberian Pyrite Belt (Schmelzbach *et al* 2007), would allow the imaging of the major fault plane rooting and simultaneously the thinning (or not) of the crust below the basin. Additional deep refraction profiles would also allow studying in more detail the thinning of the crust below the LTCB and help to establish the tectonic model for the LTCB. Together with a SGM obtained using a more detailed base of the Cenozoic map followed by gravimetric modelling that would result in a better understanding of tectonics of the study area.

Independently of the tectonic model proposed for the LTCB, seismic reflection data show that the OVLS is rooted at least to a depth of 4 km, while seismicity data suggest that it might reach 25 km depth. According to the available historical data, the 1531 event that caused widespread destruction in the capital of Portugal might have originated in the central sector

of the OVLS fault zone (e.g. Moreira 1985, Henriques *et al* 1988, Sousa *et al* 1992). Previous geological outcrop studies (Cabral *et al* 2003, 2004) and geophysical data acquired near Vila Franca (Carvalho *et al* 2006, 2009) also suggest that the central sector of the fault zone is active.

This stresses the importance of estimating maximum expected earthquakes and return periods for the OVLS. To obtain this information, the estimation of fault lengths is crucial. In spite of that the faults which separate the OVLS into its segments are presently unknown, we have a good confidence in the estimated length of the individual fault segments (or fault sectors) proposed here. Whether these fault zones are part of a single segmented structure as suggested by seismicity data and proposed in this work or individual fault zones has few implications for estimating maximum expected earthquakes, since it is generally admitted that fault zones very rarely rupture across their entire length and that ruptures occur only across fault segments.

The lack of fault outcrops in Quaternary terrains that would allow paleoseismicity studies and the absence of good quality GPS data have not allowed so far the estimation of the hazard of the active or probably active faults in the area. Therefore, maximum expected earthquakes, maximum co-seismic displacements, slip rates and recurrence intervals can only be estimated using empirical relationships like those of Wells and Coppersmith (1994) and McCalpin (2007). The following discussion on the OVLS is therefore based on these relations.

The northern sector has a total length of about 25 km and according to Wells and Coppersmith (1994) can produce a maximum earthquake of M_W 6.7 with average and maximum co-seismic displacements of 0.67 m and 1.08 m, respectively. (i) Assuming dip-slip movement on the fault, (ii) neglecting a minor strike-slip component which is known to exist in the faults with this orientation in the lower Tagus area (e.g. Cabral *et al* 2003, Vilanova and Fonseca 2004), (iii) neglecting aseismic fault slip and (iv) assuming that fault slip occurs entirely by co-seismic slip during maximum (characteristic) earthquake, we obtain a slip rate (McCalpin 2007) for this sector of 0.33 mm yr^{-1} and a maximum estimate of the average return period of approximately 2000 years.

In these calculations, we have admitted a vertical offset of 5 m across the fault at the base of the Quaternary similar to the one admitted for the central sector (Carvalho *et al* 2006). The central sector, whose total length is about 20 km, is capable of generating an event of M_W 6.6 and an average and maximum co-seismic displacement of 0.49 and 0.9 m, respectively. If we use the same empirical relationships and assumptions, we get a slip rate of 0.33 mm yr^{-1} and a recurrence interval of 1470 years.

The southern sector, the longest with a length of about 45 km, may produce an earthquake of M_W 7. Average and maximum co-seismic displacements are of 1.07 and 1.58 m, respectively. To estimate slip rates and recurrence intervals, we need to estimate the total displacement produced by the fault during a certain period of time (McCalpin 2007). Presently it is not possible to estimate this parameter for this sector of the OVLS since it is a hidden fault with a predominant strike-slip component. Using seismic reflection data, we can only estimate the total displacement produced by the small dip-slip component of the fault in the upper Miocene sediments. A value of 50 m is obtained which results in an unrealistic large value of 127 kyears for the return period.

Assumptions (i)–(iv) made above to estimate slip rates and recurrence intervals underestimate the former and overestimate the latter. In fact, the historical earthquake record on the LTV area (1344, 1531 and 1909) suggests shorter return periods for the 6–7 magnitude regional earthquakes. An explanation for the discrepancy can be, besides the above-mentioned assumptions used in the estimations, that the events have been generated by different faults that are relatively close to each other. The interaction of adjacent faults in the area would thus produce time clusters of earthquakes with events separated by recurrence intervals of the order of 10^2 years (Carvalho *et al* 2006).

6. Conclusions

The aim of this work was to investigate the LTCB and the OVLS fault zone, a recently proposed structure constituted by several regional fault zones that are known to exist in the lower Tagus valley from seismic, aeromagnetic and also geological data (Ota or Pragança fault: northern sector of the OVLS, and Vila Franca de Xira fault: central sector of the OVLS). These structures have recently been considered as a single structure, though segmented and with major importance in the regional seismotectonics framework and a possible source of most of the significant seismicity that affects the study region, delimiting a crustal domain located to the west of the structure(s) which is characterized by a higher seismic activity.

In this work, we have made the interpretation of gravimetric data using different techniques that support the previously suggested course of the OVLS fault zone. This interpretation is consistent with digital terrain models (DTM) in the northern and central sectors of the fault zone. Seismic reflection and geological data show that the OVLS in these sectors is a reverse fault with a left-lateral component that constitutes the western limit of the LTCB.

Seismicity data suggest that this structure, which separates (except the last part of the southern sector) hard rock, rugged, Mesozoic terrains of the upper western block of the reverse fault zone from softer, plain sediments of the eastern block, extends to crustal depths. It is shown here that in spite of poor hypocentre locations, it is possible to associate the down-dip prolonging of the fault surface, as seen from the seismic data in the first 4 km, with hypocentre solutions until a depth of approximately 25 km.

This conclusion is also suggested by deep refraction data collected in the northern sector. Here, the obtained velocity model is compatible with the general model of a foreland basin, and according to this model the OVLS would be the western limit of the basin accommodating major deformation. The preliminary SGM agrees with the foreland basin model and therefore supports the possibility that the OVLS reaches crustal depths. The acquisition of other deep refraction profiles in the central and southern sectors of the OVLS or/and the acquisition of deep high-resolution seismic

reflection data together with a more detailed SGM can confirm this possibility. This confirmation is extremely important for seismic hazard studies since if the OVLS is an active structure into the Quaternary, as supported by several geophysical, seismological and geological data, such a structure will be able to produce large earthquakes.

The estimation of the segment lengths made in this work, based mostly on seismic reflection and geological outcrop data, has a good accuracy and is extremely important for an appropriate evaluation of local seismic hazard. Whether the Ota fault, V. F. Xira fault and southern sector of the OVLS fault are indeed fault segments of the OVLS as proposed here or independent fault zones has no practical impact on the estimation of maximum expected magnitudes, average and maximum displacements, recurrence intervals and slip rates, since most of the times faults rupture only by segments. Therefore, preliminary maximum expected magnitudes, average and maximum displacements, recurrence intervals and slip rates have been estimated for the three sectors of the OVLS fault zone. The slip rates obtained here (0.33 mm yr^{-1}) are in agreement with the values inferred for active faults in the lower Tagus valley and other areas in Portugal mainland.

Acknowledgments

The Department of Prospecção e Exploração de Petróleos from the Direcção Geral de Geologia e Energia is gratefully acknowledged for supplying the seismic reflection data and Mohave Oil for allowing the publication of their pre-stack time migrated reprocessed data. The portuguese Foundation for Science and Technology and Projects POCTI/CTE-GIN/58250/2004 Sismotecto and PTDC/CTE-GIN/82704/2006 Sismod/Lismot is gratefully acknowledged. We are also indebted to the Centro de Geofísica da Universidade de Lisboa for several contributions to this study. We would also like to thank those who contributed to the final results presented here: Ruben Dias, Catarina Moniz, and Manuela Costa for discussions on the interpretation of the seismic reflection profiles and geodynamic implications of the results. We are particularly grateful to two anonymous reviewers for their comments and suggestions which greatly improved this work.

References

Barbosa Bernardo A P S 1995 Alostratigrafia e litostratigrafia das unidades continentais da Bacia Terciária do Baixo Tejo, Relações com o eustatismo e a tectónica *PhD Thesis* University of Lisbon 253 pp

Bielik M 1988a A preliminary stripped gravity map of the Pannonian basin *Phys. Earth Planet. Inter.* **51** 185–9

Bielik M 1988b Analysis of the stripped gravity map of the Pannonian basin *Geol. Carpathica* **39** 99–108

Bielik M, Makarenko I, Legostaeva O, Starostenko V, Dérerová J and Šefara J 2004 Stripped gravity map of the Carpathian-Pannonian basin region *Österr. Beitr. Meteorol. Geophys.* **31** 107–17

Bielik M, Makarenko I, Legostaeva O, Starostenko V, Dérerová J, Šefara J and Pašteka R 2005 New 3D gravity modeling in the Carpathian-Pannonian basin region *Contrib. Geophys. Geod.* **35** 65–78

Borges J F, Fitas A J S, Bezzeghoud M and Teves-Costa P 2001 Seismotectonics of Portugal and its adjacent Atlantic area *Tectonophysics* **337** 373–87

Cabral J 2009 Tectónica Notícia Explicativa da Folha 34-B (Loures), *Geological Map of Portugal 1/50.000,* INETI, Lisbon-Portugal

Cabral J 1995 Neotectónica em Portugal Continental *Mem. Inst. Geol. Mineiro* **31** 265

Cabral J, Moniz C, Ribeiro P, Terrinha P and Matias L 2003 Analysis of seismic reflection data as a tool for the seismotectonic assessment of a low activity intraplate basin—the Lower Tagus Valley (Portugal) *J. Seismol.* **7** 431–47

Cabral J and Ribeiro P 1988 Carta Neotectónica de Portugal Continental (escala 1:1000.000), *Map* Geological Survey of Portugal, Geology Department, Faculty of Sciences, Cabinet of Nuclear Safety and Protection

Cabral J, Ribeiro P, Figueiredo P, Pimentel N and Martins A 2004 The Azambuja fault: an active structure located in an intraplate basin with significant seismicity (Lower Tagus Valley, Portugal) *J. Seismol.* **8** 347–62

Carrilho F, Nunes J C, Pena J and Senos M L 2004 Catálogo Sísmico de Portugal Continental e Região Adjacente para o período 1970–2000 *Report* Instituto de Meteorologia ISBN 972-9083-12-6

Carvalho J 2003 Sísmica de alta resolução aplicada à prospecção, geotecnia e risco sísmico *PhD Thesis* University of Lisbon 264 pp

Carvalho J, Ghose R, Pinto C and Borges J 2009 Characterization of a concealed fault zone using P and S-wave seismic reflection data *Extended Abstracts of the EAGE Near Surface 2009/15th Meeting of Environmental and Engineering Geophysics (Dublin, Ireland, 7–9 September 2009)* p A14

Carvalho J, Cabral J, Gonçalves R, Torres L and Mendes-Victor L 2006 Geophysical methods applied to fault characterization and earthquake potential assessment in the Lower Tagus Valley, Portugal *Tectonophysics* **418** 277–97

Carvalho J, Matias H, Torres L, Manupella G, Pereira R and Mendes-Victor L 2005 The structural and sedimentary evolution of the Arruda and Lower Tagus sub-basins, Portugal *Mar. Pet. Geol.* **22** 427–53

Carvalho J, Taha R, Cabral J, Carrilho F and Miranda M 2008 Geophysical characterization of the Ota-Vila Franca de Xira-Lisbon-Sesimbra fault zone, Portugal *Geophys. J. Int.* **174** 567–84

Cobbold P R, Davy P, Gapais D, Rossello E A, Sadybakasov E, Thomas J C, Tondji Biyo J J and de Urreiztieta M 1993 Sedimentary basins and crustal thickness *Sedimentary Geol.* **86** 77–89

Cooper G R J and Cowan D R 2003 Applications of fractional calculus to potential field data *Explor. Geophys.* **34** 51–6

Curtis M 1999 Structural and kinematic evolution of a Miocene to recent sinistral restraining bend: the Montejunto massif, Portugal *J. Struct. Geol.* **21** 39–54

Dineva S, Batlló J, Mihaylov D and van Eck T 2002 Source parameters of four strong earthquakes in Bulgaria and Portugal at the beginning of the 20th century *J. Seismol.* **6** 99–123

Domzalski W 1969 Interpretation of an aeromagnetic survey offshore Portugal (1:200.000) *Report* Fairey Surveys Ltd, Maidenhead, Berkshire, England

Dooley T P, Monastero F C and McClay K R 2007 Effects of a weak crustal layer in a transtensional pull-apart basin: results from a scaled physical modeling study *American Geophysical Union, Fall Meeting 2007* abstract no V53F-04

GM-SYS 1995 Gravity and magnetic modelling version 3.6, Northwest Geophysical Association, Inc. (NGA), OR, USA

GPEP (Gabinete para a Pesquisa e Exploração de Petóleos) 1986 *Petroleum Potential of Portugal* (Lisboa: GPEP) p 62

Grant F S and West G F 1965 *Interpretation Theory in Applied Geophysics* (New York: McGraw-Hill)
Hammer S 1963 Deep gravity interpretation by stripping *Geophysics* **28** 369–78
Henriques M C, Mouzinho M T and Ferrão N M 1988 *Sismicidade de Portugal. O Sismo de 26 de Janeiro de 1531* (Portugal: Comission for the National Earthquake Catalogue) 100 pp
Hsu S-K 2002 Imaging magnetic sources using Euler's equation *Geophys. Prospect.* **50** 15–25
Justo J L and Salwa C 1998 The 1531 Lisbon earthquake *Bull. Seismol. Soc. Am.* **88** 319–28
Legostaeva O 2000 On optimal scheme of computing double integrals in solving direct gravimetric and magnetometric problems *Geophys. J.* **19** 693–9
Leinfelder R R and Wilson R C L 1998 Third-order sequences in an Upper Jurassic rift-related second-order sequence, Central Lusitanian Basin, Portugal *Mesozoic and Cenozoic Sequence Stratigraphy of European Basins* ed P C Graciansky, J Hardenbol, T Jacquin and P R Vail (Tulsa, OK: SEPM Special Publication 60) pp 507–25
Lienert B, Berg E and Neil Frazer L 1986 Hypocenter: an earthquake location method using centered, scaled and adaptively damped least squares *Bull. Seismol. Soc. Am.* **76** 771–83
Lienert B and Havskov J 1995 A computer program for locating earthquakes both locally and globally *Seismol. Res. Lett.* **66** 26–36
Linsser H 1967 Investigation of tectonic by gravity detailing *Geophys. Prospect.* **15** 480–515
LNEG 2010 Geological Map of Portugal, scale 1: 1.000.000, Laboratório Nacional de Energia e Geologia, Ministry of Economy, Innovation and Development, Alfragide
Matias L 1996 A sismologia experimental na modelação da estrutura da crusta em Portugal continental *PhD Thesis* University of Lisbon 398 pp
McCalpin J P 2007 *Paleoseismology* (New York: Academic)
Mendes-Victor L A, Hirn A and Veinant J L 1980 A seismic section across the Tagus Valley, Portugal: possible evolution of the crust *Ann. Geophys.* **36** 469–76
Moreira V S 1985 Seismotectonics of Portugal and its adjacent area in the Atlantic *Tectonophysics* **117** 85–96
Moreira V S, Prodehl C, Mueller St and Mendes A S 1980 Crustal Structure of Western Portugal *Proc. 17th Assembly of the ESC (Budapest)* pp 529–32
Mueller S, Prodehl C, Mendes A S and Moreira V S 1973 Crustal structure in the southwestern part of the Iberian peninsula *Tectonophysics* **20** 307–18
Oliveira T (coord.) *et al* 1992 Carta Geológica de Portugal, escala 1: 500.000, *Map*, Serviços Geológicos de Portugal, Lisboa
Peláez J A M, Casado C L and Romero J H 2002 Deaggregation in magnitude, distance, and azimuth in the south and west of the Iberian peninsula *Bull. Seismol. Soc. Am.* **92** 2177–85
Rasmussen E S, Lomholt S, Anderson C and Vejbaek O V 1998 Aspects of the structural evolution of the Lusitanian Basin in Portugal and the shelf and slope area offshore Portugal *Tectonophysics* **300** 199–225
Reid A B, Allsop J M, Granser H, Millett A J and Somerton I W 1990 Magnetic interpretation in three dimensions using Euler deconvolution *Geophysics* **55** 80–91
Ribeiro A 2002 *Soft Plate and Impact Tectonics* (Berlin: Springer) 324 pp
Ribeiro A, Cabral J, Baptista R and Matias L 1996 Stress pattern in Portugal mainland and the adjacent Atlantic region, West Ibéria *Tectonics* **15** 641–59
Ribeiro A, Kullberg M C, Kullberg J C, Manupella G and Phipps S 1990 A review of Alpine tectonics in Portugal: foreland detachment in basement and cover rocks *Tectonophysics* **184** 357–66
Schmelzbach C, Juhlin C, Carbonell R and Simancas J F 2007 Prestack and poststack migration of crooked-line seismic reflection data: a case study from the South Portuguese Zone fold belt, southwestern Iberia *Geophysics* **72** B9–18
Sousa M L, Matins A and Oliveira C S 1992 Compilação de Catálogos Sísmicos da Região Ibérica *Report 36/92* NDA, Dept Estruturas, Núcleo Dinâmica Aplicada, Proc. 036/11/9295, LNEC, Lisboa
Starostenko V I, Matsello V V, Aksak I N, Kulesh V A, Legostaeva O V and Yegorova T P 1997 Automation of the computer input of images of geophysical maps and their digital modelling *Geophys. J.* **17** 1–19
Stavrev P Y 1997 Euler deconvolution using differential similarity transformations of gravity or magnetic anomalies *Geophys. Prospect.* **45** 207–46
Stich D, Batlló J, Macià R, Teves-Costa P and Morales J 2005 Moment tensor inversion with single-component historical seismograms: the 1909 Benavente (Portugal) and Lambesc (France) earthquakes *Geophys. J. Int.* **162** 850–8
Surinkum A 1989 Geological interpretation of airborne and ground magnetic survey *Master Thesis* University of Western Ontario, Canada pp 34–40
Talwani M 1965 Computation with the help of a digital computer of magnetic anomalies caused by bodies of arbitrary shape *Geophysics* **30** 797–817
Teves-Costa P, Rio I, Marreiros C, Ribeiro R and Borges J F 1999 Source parameters of old earthquakes: semi-automatic digitalization of analog records and seismic moment assessment *Nat. Hazards* **19** 205–20
Thompson D T 1982 EULDPH—a new technique for making computer-assisted depth estimates from magnetic data *Geophysics* **47** 31–7
Vilanova S P and Fonseca J F B D 2004 Seismic hazard impact of the Lower Tagus Valley Fault Zone (SW Iberia) *J. Seismol.* **8** 331–45
Wells D L and Coppersmith K J 1994 New empirical relationships among magnitude, rupture length, rupture width, rupture area and surface displacement *Bull. Seismol. Soc. Am.* **84** 974–1002
Westerhausen H 1956 Report on reflection and refraction seismic investigations carried out in South Tejo Basin for Companhia dos Petróleos de Portugal and Mobil Exploration Company Lisboa (Portugal) by Prakla 20 pp
Wilson R C L, Hiscott R N, Willis M G and Gradstein F M 1989 The Lusitanian Basin of west central Portugal: Mesozoic and Tertiary tectonics, stratigraphy and subsidence history *Extensional Tectonics and Stratigraphy of the North Atlantic Margins (American Association Petroleum Geologists Memoir* vol 46*)* ed A J Tankard and H Balkwill (Tulsa, OK: American Association of Petroleum Geologists) pp 341–61